PolyOculus: Simultaneous Multi-view Image-based Novel View Synthesis

Jason J. Yu[1,3]   Tristan Aumentado-Armstrong[1,2,3]   Fereshteh Forghani[1]

Konstantinos G. Derpanis[1,3]   Marcus A. Brubaker[1,3]

[1]York University   [2]University of Toronto   [3]Vector Institute for AI

{jjyu,forghani,kosta,marcus.brubaker}@yorku.ca,   taumen@cs.toronto.edu

Abstract

This paper considers the problem of generative novel view synthesis (GNVS), generating novel, plausible views of a scene given a limited number of known views. Here, we propose a set-based generative model that can simultaneously generate multiple, self-consistent new views, conditioned on any number of known views. Our approach is not limited to generating a single image at a time and can condition on zero, one, or more views. As a result, when generating a large number of views, our method is not restricted to a low-order autoregressive generation approach and is better able to maintain generated image quality over large sets of images. We evaluate the proposed model on standard NVS datasets and show that it outperforms the state-of-the-art image-based GNVS baselines. Further, we show that the model is capable of generating sets of camera views that have no natural sequential ordering, like loops and binocular trajectories, and significantly outperforms other methods on such tasks.

1. Introduction

This paper considers the problem of generating novel, plausible views of a scene given a limited number of known views, also known as novel view synthesis (NVS). We propose a novel formulation of the problem that is able to generate a variable number of new views given any number of known views. Unlike previous work in this space, our approach is not limited to generating a single image at a time and can condition on zero, one, or more views. As a result, when generating a large number of views, our method is not restricted to a low-order autoregressive generation approach and is better able to maintain generated image quality over large sets of images. Further, it allows for the generation of sets of camera views that have no natural sequential ordering, like loops and binocular trajectories.

Novel view synthesis (NVS) generally aims to predict scene appearance from new perspectives, given multiview posed images. *Generative* NVS (GNVS) is more general:

for instance, given a single image of a hallway with an unobserved room, can we generate plausible novel views from *inside* the room? This becomes a conditional generative modeling problem, asking for images that match the previously observed views and their implied 3D scene structure. Existing work is either limited in its extrapolative capacity (e.g., cannot move the camera arbitrarily) or suffers from cross-view inconsistency (i.e., scene changes occur between generated frames). In this work, we mitigate the latter problem without incurring the former limitation by pinpointing and addressing a significant issue with the ordered autoregressive approach that characterizes existing image-based GNVS models. Our primary innovation is a reformulation of the model as *set-to-set* generation, meaning we condition on a set of zero or more posed images to generate a set of output views in a simultaneous and self-consistent manner. The resulting model outperforms existing models in terms of image quality and also removes a fundamental yet previously unquestioned assumption about the ordered nature of viewpoint trajectories. By removing this assumption, our set-based method particularly improves performance on trajectories where a natural ordering is unclear.

NVS scenarios form a continuum between the more common well-determined case, where minimal ambiguity exists, and the GNVS case, which is closer to standard generative image modeling. This is largely decided by the number of available observations and their relation to the desired views (i.e., their proximity in camera position and orientation). In the well-determined case, scene content has significant coverage from disparate viewpoints (relative to the target view distribution), providing powerful constraints on the 3D scene structure and effectively enabling synthesis via a 3D-aware interpolation between views. This is the typical scenario for standard Neural Radiance Fields (NeRFs) [29], which often focuses on cases with many known views and significant overlap between observed and synthesized views. In contrast, the problem is much more ill-posed when as few as one observation is given, or if the model is queried for a viewpoint far from the distribution of known views. In such cases, the space of plausible novel views is

Figure 1. An illustrative example of a "loop inconsistency" in which an image-based generative NVS network fails to retain consistency with its previous generations, and its resolution with a set-based approach. We show the starting observation (i.e., real-image), from which the sequence of novel views is synthesized, on the upper-left; below it, we depict the trajectory that the camera follows (a "spinning" motion pointed at a fixed visual target). Notice that such a trajectory causes some parts of the scene to be hidden (i.e., occluded), and then reappear later. Using an autoregressive strategy (top row) causes the network to forget its previous generations and invent inconsistent scene content (e.g., compare final column images to the observation, particularly in the marked areas). In contrast, our set-based method (bottom row) is able to construct a self-consistent set of views by (i) more intelligent conditioning on the most relevant set of images and (ii) simultaneous generation of multiple views in a set, allowing mutual constraints within the sampling process.

very large due to uncertainties caused by occlusions, lack of viewpoint coverage, and depth ambiguities; hence, generative models are a natural choice for representing this uncertainty. Herein, we focus on the GNVS problem.

As conditional generative models increase in both quality and scope of applicability (e.g., see [12, 31]), interest in GNVS models has concomitantly surged (e.g., [1, 9, 27, 35, 36, 47, 49, 50, 52, 57]), utilizing various forms and levels of inductive biases. Rendering-based methods [1, 9, 47, 49] first sample an explicit 3D representation of the scene, which is then rendered to novel views. Such views are 3D consistent by design but can be limited by the spatial bounds of the representation. In contrast, image-based models [27, 35, 36, 50, 52, 57] approach NVS as an image-to-image problem without the use of strong 3D priors. These methods are not spatially bounded but require the model to learn 3D consistency from multiview data. Such approaches typically use (first order) autoregressive sampling to generate longer trajectories through a scene where images are generated one at a time and typically conditioned on only a single other known view. However, this first order autoregressive approach (i) accumulates errors over longer generations, (ii) creates inconsistencies between near-viewpoint generations due to divergent conditioning histories (e.g., when generating a sequence that loops back to its start), and (iii) requires an ordering of the views which may not naturally exist (e.g., with loops and polyocular trajectories). Fig. 1 provides an illustration of these issues, particularly (i) and (ii). We propose using set-

based view generation, which avoids these issues by formulating the generative model to jointly sample multiple self-consistent images simultaneously and conditioned on multiple known views.

In this paper, we propose a novel pose-conditional diffusion model for GNVS, which operates in a set-to-set manner. Specifically, our model can (a) condition on a variable number of views (≥ 0) in a permutation-invariant manner, and (b) generate a set of novel views with neither order-dependence nor fixed cardinality. Further, while our model is theoretically capable of simultaneously generating and conditioning on any number of views, there are practical constraints due to limited memory and computation. Hence, we propose a hybrid generation strategy that avoids the practical limitations. The use of multiview conditioning (a) allows for stronger constraints of the generated images, leading to more consistent output views. Similarly, *simultaneous* generation of a large view-set (b) can be performed using our method in a *mutually self-constraining* manner, which reduces error accumulation over long trajectories (i) and, with a novel hybrid sampling strategy, avoids inconsistencies even with very large view sets (ii). We show empirically that these alterations greatly improve image quality and result in much higher-quality generated views. Further, we show that the generation of view-sets *without* a natural ordering significantly benefits from our set-based approach, compared to the arbitrary imposition of an ordering.

Autoregressive Dependency

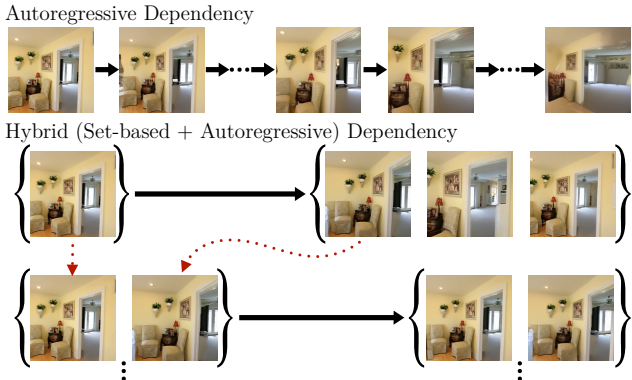Hybrid (Set-based + Autoregressive) Dependency

Figure 2. Depiction of the differing dependency structure between our hybrid sampling strategy (which balances stronger constraints with computational efficiency) and standard autoregression. We show generations of single views or view-sets with black arrows. For the set-based case, the dotted lines show the structure of the conditioning frames in the next step. Our hybrid approach is able to immediately synthesize consistent frames from diverse viewpoints, within the first set. This initial set can then provide more powerful constraints on the generative model in later steps, preventing the divergence seen in the top row (see also Fig. 1).

2. Related Works

Novel View Synthesis (NVS). Constructing new views of scenes from multiview images has a long history in computer vision and graphics (e.g., [3, 11, 24, 41, 43]). Such NVS techniques roughly span two axes: (i) image-based vs. geometry-based rendering (how much geometry is necessary [10, 44]) and (ii) interpolative vs. generative synthesis (how much *extrapolation* is used). Neural Radiance Fields (NeRFs), a recent interpolative method, renders with a learned implicit 3D geometry (e.g., [4, 16, 29, 53]); however, it not only relies on per-scene optimization, but it is also unable to generate realistic details in unseen areas. Our work, in contrast, eschews inferring scene geometry, as it entails solving an ill-posed problem that may not necessarily be required to obtain realism or consistency. Further, we focus on the *generative* case, where the model is tasked to indefinitely extend the scene from minimal initial information (e.g., a single image). Existing works that generate 3D structure directly, including geometry, generally have limited scene extents, prohibiting indefinite spatial extension (e.g., [5, 23]). More recent methods combine 3D structure with autoregressive generation to enable extrapolation. Tewari et al. [49] combine a generalizable NeRF [56] with a diffusion model, but sampling is very costly in time and memory, while GeNVS [9] utilizes a 3D feature volume to condition a diffusion model. Due to computational cost, these methods are limited in resolution compared to ours.

Our work is most similar to *image-based* GNVS methods, generally based on pose-aware conditional diffusion models. Zero-123 [13, 27], 3DiM [52], Viewset-Diffusion [47], and RenderDiffusion [1] focus on object-centric NVS, whereas our method operates on full scenes and enables indefinite extrapolation. In the scene-centric domain, Ge-oGPT [36], LookOut [35], PhotoCon [57], and Tseng et al. [50] generate autoregressive sequences; however, while scene structure is coarsely preserved, dramatic changes can still occur across frames. Video generative models struggle with similar challenges (e.g., [6, 17]), albeit without the 3D aspects of the problem. These methods suffer from error accumulation across trajectories and "loop inconsistencies" (where returning to the same viewpoint does not preserve previously observed structure), induced by the pose ordering. We show that a set-based approach can substantially mitigate such issues.

Set-Theoretic Learning. Set-valued data underlie numerous problems in computer vision, such as point cloud processing (e.g., [2, 32, 33]), anomaly detection (e.g., [25, 34]), feature matching (e.g., [40]), and few-shot learning (e.g., [54]), necessitating in/equivariance to permutation and cardinality [42, 58, 62]. Similarly, many problems are naturally formulated as set prediction tasks, including object detection [7, 18], shape generation (e.g., [22, 28]), and vector graphics representations [8]. For NVS, while prior work considered set-based latent encodings [39], it did not examine set-structured simultaneous generation.

In this work, we operate in a *set-to-set* manner by generating a set of NVs, given a set of conditioning images. Unlike autoregression, this avoids imposing an arbitrary ordering onto the set, which can cause difficulties in the general case [60, 61]. For instance, consider sequences of polyocular frames (e.g., binocular, to mimic humans, or higher-order, for the multicamera setups common in autonomous driving [55] and elsewhere [15]) – within each polyocular set, there is no single natural ordering. Other common distributions, such as sets of inward-facing cameras around an object, are difficult to order as well. Finally, autoregressive methods (e.g., [26, 35, 36, 57]) often accumulate errors over trajectories or incur inconsistencies at identical cameras arrived at via different paths. In contrast, by generating *sets* of frames, we can devise a novel hybrid sampling approach that mitigates such divergences (see Fig. 2).

3. Technical approach

In this section, we first briefly review relevant background on diffusion models, then describe our set-based multi-view diffusion model, and finally detail methods for practically sampling large novel view-sets using our model.

3.1. Background

Diffusion models [20, 45, 46] are a class of generative models where the generative process is formulated as the reverse

3

of a fixed forward noising process. Given a data sample drawn from $q(\mathbf{x}_0)$, a typical Gaussian forward process is discretized into $t \in \{0, \ldots, T\}$ steps, which are defined via

$$q(\mathbf{x}_t|\mathbf{x}_{t-1}) = \mathcal{N}(\mathbf{x}_t; \sqrt{1 - \beta_t}\mathbf{x}_{t-1}, \beta_t\mathbf{I}), \qquad (1)$$

where $\mathbf{I}$ is the identity matrix, and the coefficients, β_t, parameterize the forward process such that $\mathbf{x}_t$ is approximately normal when $t \approx T$. The reverse process is also Gaussian at each step but relies on learned parameters, θ:

$$p_\theta(\mathbf{x}_{t-1}|\mathbf{x}_t) = \mathcal{N}(\mathbf{x}_{t-1}; \mu_\theta(\mathbf{x}_t, t), \beta_t\mathbf{I}), \qquad (2)$$

where μ_θ estimates the mean of the reverse step. This can be reparameterized using the noise estimator, $\epsilon_\theta(\mathbf{x}_t, t)$:

$$\mathbf{x}_{t-1} = \frac{1}{\sqrt{\alpha_t}}\left(\mathbf{x}_t - \frac{1 - \alpha_t}{\sqrt{1 - \bar{\alpha}_t}}\epsilon_\theta(\mathbf{x}_t, t)\right) + \beta_t\zeta_t \qquad (3)$$

where $\alpha_t = 1 - \beta_t$, $\bar{\alpha}_t = \prod_{s=1}^{t} \alpha_s$, and $\zeta_t \sim \mathcal{N}(0, \mathbf{I})$. Samples are drawn by starting from standard normal $\mathbf{x}_T$ and progressively denoising the image using Eq. 3. Conditional generation involves providing additional inputs to ϵ_θ, which remain constant throughout the reverse process.

To reduce computational requirements, we use a latent diffusion model [30, 37] that maps the data into a latent space, $\mathbf{z} = \mathrm{E}(\mathbf{x})$, with reduced dimensionality. The diffusion model is learned in the latent space, and data is decoded back to image space via the decoder, $\mathbf{x} = \mathrm{D}(\mathbf{z})$. For our application, the autoencoder is fully convolutional to preserve the spatial structure of images.

3.2. Set-based NVS Diffusion Model

We begin by considering the the distribution over sets of N views, conditioned on their camera poses, $\mathbf{c} = \{\mathbf{c}_1, \mathbf{c}_2, \ldots, \mathbf{c}_N\}$:

$$p_\theta(\{\mathbf{z}_1, \mathbf{z}_2, \ldots, \mathbf{z}_N\}|\mathbf{c}), \qquad (4)$$

where $\mathbf{z}_n$ is the latent representation for view $n \in \{1, \ldots, N\}$. Critically, this distribution should be permutation invariant since there may not be any natural ordering amongst the views. Additionally, since the choice of global coordinates is arbitrary (i.e., only relative camera poses are meaningful), the distribution should be invariant to global rigid transformations of the camera poses, $\mathbf{c}$.

To construct such a *set-based* diffusion model, we take inspiration from previous generative NVS methods [52, 57], as well as video diffusion models [21], where separate streams of the model provide the noise estimate of each image. Specifically, each view is processed by a U-Net [38] with shared weights, which only communicates between streams via attention layers, while the remaining layers operate on each view independently. Since attention layers are permutation-equivariant by design, we can construct an
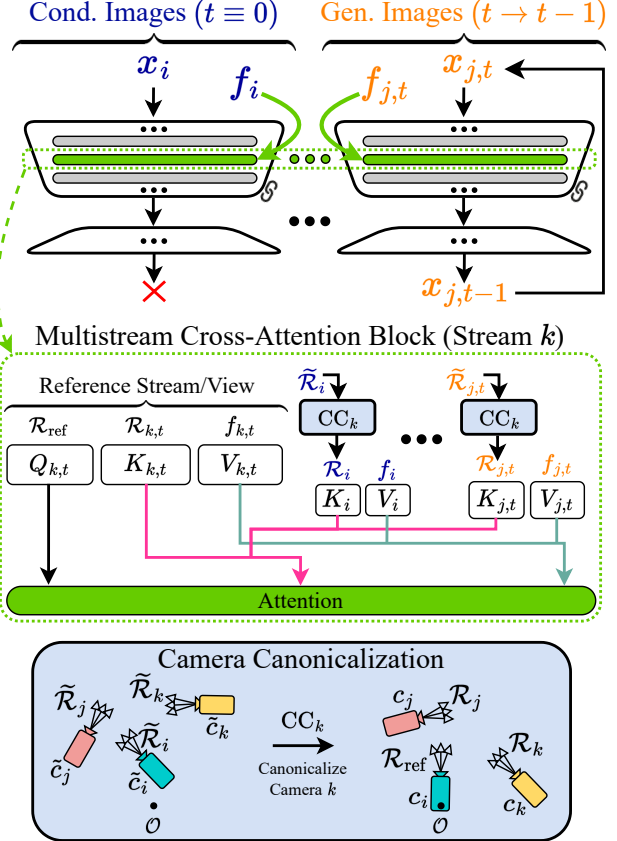

Figure 3. U-Net architecture for set-based NVS. Given a set of conditioning images, $X_c = \{x_1, \ldots, x_{n_c}\}$, we generate a set of novel views, $X_{g,t} = \{x_{n_c+1,t}, \ldots, x_{n_c+n_g,t}\}$, via a reverse diffusion process. A fixed time conditioning at $t \equiv 0$ is used for X_c (i.e., no noise is added), but processing is otherwise identical compared to $X_{g,t}$. A multistream approach enables simultaneous generation, where the U-Net is independently applied (i.e., with shared parameters) to each $x \in X_c \cup X_{g,t}$, except at cross-attention (CA) layers, which facilitate order-independent inter-stream mutual dependency. Specifically, each CA block combines information from (i) same-layer features ($f_{j,t}$) and (ii) camera information ($\widetilde{c}_j$, with associated rays $\widetilde{\mathcal{R}}_j$) across all other streams j. To obtain the output of the ith stream, while ensuring invariance to global rigid scene transforms, a *camera canonicalization block*, CC_i, is applied to the rays: $\mathcal{R}_j = \mathrm{CC}_i(\widetilde{\mathcal{R}}_j)$, which transforms $\widetilde{c}_i$ to the origin, $\mathcal{O}$, with a canonical orientation. Then, for stream i, the queries, $Q_{i,t}$, are given by the reference rays, $\mathcal{R}_{\mathrm{ref}}$, while the keys and values are given by the transformed rays, $\{\mathcal{R}_j\}_j$, and features, $\{f_{j,t}\}_j$, respectively, across all streams j.

ordering-independent noise estimator over sets of noisy latents, along with their camera poses:

$$\epsilon_\theta(\{(\mathbf{z}_{1,t}, \mathbf{c}_1), \ldots, (\mathbf{z}_{N,t}, \mathbf{c}_N)\}, t). \qquad (5)$$

Since reasoning about the scene across views relies deeply on knowledge of the (relative) camera geometry, the mecha-

nism by which such information is injected into the generative process must be carefully designed. In particular, camera poses are used to modulate the attention layers by injecting a camera ray representation into the keys and queries. We adopt an image-based representation of camera rays, where per-pixel ray directions (determined by the camera parameters) are assembled into an array, followed by a fixed frequency-based Fourier encoding [48] (e.g., see [39, 57]; non-image-based NVS methods, such as NeRFs, utilize a similar representation as well). However, since only the relative camera poses are meaningful, we *canonicalize* the rays used by the attention block in each stream, such that the camera of the view processed by that stream is positioned at the origin with no rotation. This enables mutually constrained generation (i.e., with each stream informed of each other) of arbitrary-sized sets in a permutation-invariant manner, while maintaining invariance to global rigid transforms. The most similar method to ours, by Yu et al. [57], considered only the two-stream case, with one image acting as a fixed observation. Our architecture, including the canonicalized rays, is illustrated in Fig. 3.

While our model is capable of sampling without conditioning on scene information via Eq. 4, the primary cases of interest in generative NVS involve conditioning on observed (or previously synthesized) frames. To account for this, our model defined in Eq. 5 can also be conditioned on observed views, using a small modification to the noise estimator:

$$\epsilon_\theta(\{(\mathbf{z}_{1,t}, \mathbf{c}_1, t_1), \dots, (\mathbf{z}_{N,t}, \mathbf{c}_N, t_N)\}), \qquad (6)$$

where the time conditioning for all the views, t, is replaced with a separate time conditioning, t_n, for every view $\mathbf{z}_n$. Then, the model can flexibly treat inputs with $t_n = 0$ as conditioning views, similar to previous work [47]. Such views are not noised by the diffusion model; hence, they act as constant conditioning factors across the generative process.

3.3. Sampling Large Sets of Views

In principle, our model can operate over an arbitrarily large number of views. However, doing so in practice may be limited by the computational constraints caused by the quadratic time complexity of attention with respect to the number of views. For these reasons, it is still desirable to be able to generate views autoregressively. However, instead of generating a single view at a time, our model can generate and condition on sequential sets of views. By carefully selecting the sets and their order of generation, our model can minimize image quality deterioration during autoregressive generation, and improve consistency for sets of views where there is no natural ordering. In other words, for tractability, we can sample with a "hybrid" strategy, which uses autoregressive generation of sets of views, conditioned
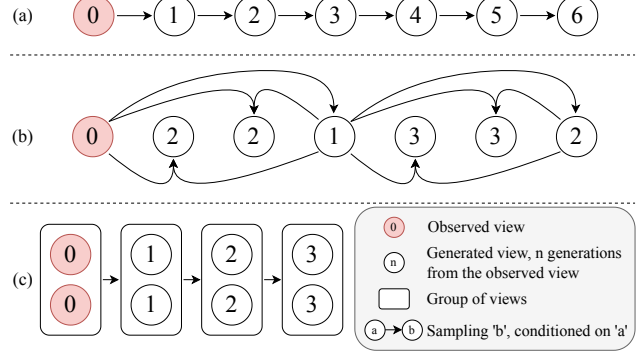

Figure 4. Different generation orders, and the depth of each view from the observed image. We show the depth of each view from the observed view(s) in red for (a) standard autoregressive sampling, (b) keyframed sampling, and (c) grouped sampling. Notice that the view(s) with the largest depth when sampling with (b) and (c) grows slower with respect to the total number of views, than with (a) standard autoregressive sampling. This reduces the accumulation of errors in later views.

of sets of selected views. Selecting an appropriate conditioning hierarchy (i.e., which view-sets to output together, and which to use for conditioning at each stage) is thus a new design space for our model.

Specific sets of views, such as those along a linear camera trajectory, have a natural ordering that is amenable to standard autoregressive sampling used by previous methods (e.g., [35, 36, 49, 50, 57]). These methods can generate an arbitrary number of views by conditioning successive generations on previous ones. The factorized generation distribution over all views is:

$$p(\mathbf{z}_1, \dots, \mathbf{z}_N) = p(\mathbf{z}_1) \prod_{n=2}^{N} p(\mathbf{z}_n | \mathbf{z}_{n-1}). \qquad (7)$$

For the remainder of this paper, we omit the dependence on the camera poses, $\mathbf{c}$, for clarity. A drawback of this method is the accumulation of errors over successive generations since views generated later in the sequence are conditioned on previous frames that may include errors themselves. Further, by only considering the most recent frames, it is possible for the model to *forget* previously constructed parts of the scene – such errors can lead to "loop inconsistencies", in which frames generated for nearby cameras at different times do not match, due to different conditioning histories. While stochastic conditioning (e.g., [50, 52]) has been proposed, in part to reduce this issue, it can be challenging to use in practice (e.g., [57]).

One way to reduce the error in the generated views is to reduce the "depth" of the autoregressive dependencies of the views. Suppose we imagine a directed graph where nodes are images and directed edges represent conditional generations. In that case, the depth of a generated view

5

is the minimum path length from the real observed initial frame. A generation at high depth is, therefore, far from the original conditioning input and, in image-based GNVS models, liable to "forget" its constraints. The graph for first-order autoregressive generation is a chain; hence, its maximum depth is equal to the number of views.

In general, let $\mathcal{V}_1, \ldots, \mathcal{V}_G$ be a non-overlapping sequential partition of all views to be generated and $\mathcal{C}_i$ be the set of views to be conditioned on when generating $\mathcal{V}_i$ such that $\mathcal{C}_i \subseteq \cup_{j=1}^{i-1} \mathcal{V}_j$, which ensures feasibility of the ordering. Generation based on these sets can then be described as

$$p(\mathbf{z}_1, \ldots, \mathbf{z}_N) = \prod_{i=1}^{G} p(\{\mathbf{z}_j | \forall j \in \mathcal{V}_i\} | \{\mathbf{z}_k | \forall k \in \mathcal{C}_i\}). \quad (8)$$

The maximum depth of such a generation strategy is at most G and could be less. For instance, $\mathcal{V}_1$ could generate a set of regularly spaced "keyframes", and subsequent $\mathcal{V}_i$ would generate the in-between frames, conditioned only on neighbouring keyframes, which could have a maximum depth as low as two.

In cases where there is no inherent or natural ordering of views, the concept of keyframes may not be directly applicable; similar strategies can be used. For example, if a trajectory of stereo pairs is desired, then keyframe pairs can be considered. Alternatively, if the generation of a cloud of views is needed, then the initial "keyframes" may be selected as evenly distributed among the set of views based upon their camera extrinsics, and "in-between" frames can be generated conditioned on their nearest, previously generated keyframes. There are a multitude of generation strategies that our model can support in order to manage the computational burden of generation while still minimizing depth. See Figure 4 for an illustration of some sampling strategies and the concept of generation depth. We explore different generation strategies in the experimental section and provide further details in the appendix.

4. Results

4.1. Experimental setup

We evaluate on the RealEstate10K dataset [63], which contains real-world multiview image sets derived from videos. The scenes provide rich, structured data with relatively large extents and camera motions, and have been commonly used by related prior works (e.g., [35, 36, 51, 57]). We use an image size of 256×256, derived from center crops. Additional experimental results are available in the appendix.

Building on the architecture of previous works [57], our method is implemented as a latent diffusion model [37], based on a VQ-GAN autoencoder [14]. During training, for a given scene, we uniformly randomly select $n \sim \mathcal{U}([1, \ldots, 5])$ total views, then set $n_c \sim \mathcal{U}([0, \ldots, n-1])$ of them to act as conditioning images (which have fixed

$t \equiv 0$; see Fig. 3). We utilize the standard DDPM noising process [20], with a modified loss that considers only non-conditioning views (i.e., the $n - n_c$ generated views).

We evaluate on NVS, using the experimental settings of prior work (e.g., [35, 36, 57]). We compare primarily to the state-of-the-art method PhotoCon [57]. Further, while our method is trained in a set-based manner, it is also capable of autoregressive generation, as in prior works. Therefore, we operate our model using this sampling approach as well, which serves to quantify the utility of our novel sampling approach. We refer to standard autoregression as the one-step Markov case; however, for tractability, our hybrid approach sometimes also generates sets sequentially (e.g., for initial keyframe generation), often via frames of varying "depth" from the starting frame (see Sec. 3.3). We denote this as *set-autoregression*, as each step conditions on a set of views and also outputs a set of views.

Three metrics are used to quantify performance: (i) when ground-truth sequences are available, we compute reference-based image quality via PSNR and LPIPS [59]; (ii) FID [19], which measures image quality or realism; and (iii) thresholded symmetric epipolar distance (TSED) [57], which quantifies *consistency* between views. Briefly, TSED is computed over pairs of views with the known camera poses; matched features between the two frames are used to measure error with respect to their expected epipolar geometry; image pairs with both sufficient matches ($\geq T_{\text{matches}}$) and low enough median error ($< T_{\text{error}}$) are counted as consistent, and the metric overall counts the proportion of consistent frames.

4.2. Keyframed generation on sequential views

We first evaluate our method using standard autoregressive and keyframed sampling strategies for sequential view generation on RealEstate10K. Following previous work (e.g., [35, 36, 57]), we evaluate using in-distribution trajectories taken from the test split of the data. Further, as in [57], we consider an out-of-distribution camera trajectory, denoted "spin", which is of particular interest as it often displays "loop inconsistencies" with standard autoregression (e.g., see Fig. 1). In-distribution trajectories with at least 200 available frames are considered, and subsampled such that we generate 20 views per sequence. For keyframed generation, we first set-autoregressively generate keyframes spaced two views apart along the sequence. The remaining frames are then generated in groups while conditioned on the two closest keyframes. With the known ground-truth frames for in-distribution trajectories, we perform standard reference-based evaluations in image space. We consider the fifth and final generated images as short-term and long-term, respectively. As shown in Tab. 1, over both timescales, our model with keyframed sampling has superior performance, compared to both PhotoCon and our model
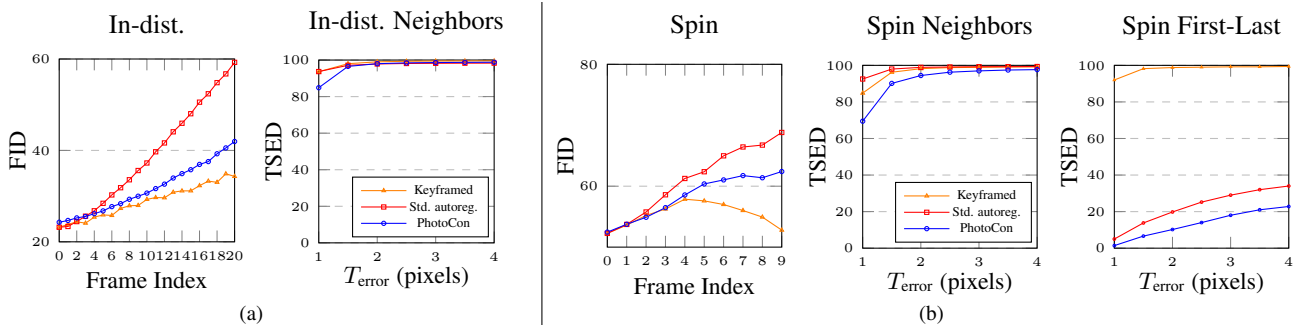
Figure 5. (a) FID and TSED plots for in-distribution trajectories. (b) FID and TSED plots for the spin trajectory, which is cyclical, and a TSED plot comparing the first and last frames.

Table 1. RealEstate10K reconstruction on in-distribution poses.

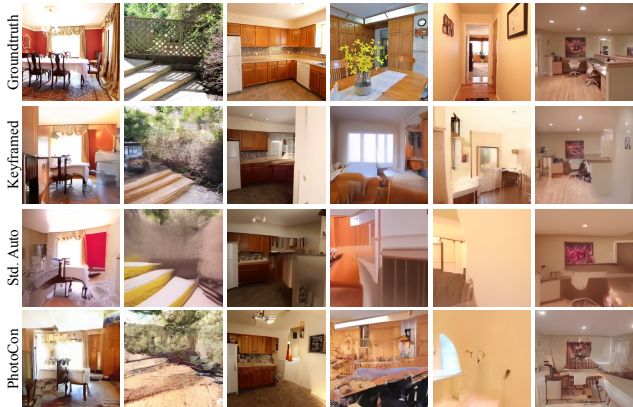| Method	Short-term		Long-term	
	LPIPS ↓	PSNR ↑	LPIPS ↓	PSNR ↑
PhotoCon [57]	0.333	15.51	0.588	11.54
Ours-auto.	0.325	15.35	0.623	11.45
Ours-keyf.	**0.306**	**15.79**	**0.575**	**11.76**

Figure 6. Qualitative examples of the last frames of generated sequences on in-distribution trajectories. Notice the quality of the images generated using the keyframe method is higher than the other methods.

with standard autoregressive sampling.

To evaluate the degradation of image quality as views are successively generated, we evaluate FID between the generated views at each time-step and a fixed set of random test views. Quantitative results in Fig. 5a (left) show that FID tends to deteriorate as trajectories grow, but our keyframed strategy substantially mitigates this degradation, compared to the other methods, giving us the best image quality. The reduced degradation from keyframing can be observed qualitatively in Fig. 6; We also note that our approach does not sacrifice inter-frame consistency to obtain this improvement (see Fig. 5a, right), according to TSED. Thus, keyframing with our set-based model increases image quality while maintaining consistency, compared to prior work [57] or standard autoregressive sampling.

Loop closure. We next examine a particular out-of-distribution trajectory, the spin, which illustrates the "loop inconsistency" problem, while also challenging the generalization capabilities of the model. In this case, our keyframe approach generates an initial frame-set that maximizes inter-camera distance (see Sec. 3.3 and the appendix for details). In this way, we can generate cyclical trajectories where the start and end frames should be consistent, since frames near the end have low generation depth. However, this is difficult for standard autoregressive methods since the conditioning may be insufficiently informative about the earlier history of the trajectory to enable cycle-consistency (i.e., the generation depth is too high).

We display our results in Fig. 5b. First, consider the per-frame FID (left inset): while all methods perform similarly close to the initial view, our approach exhibits an interesting parabolic behaviour where FID peaks and then decreases, even as error continues accumulating for the other models. This is due to the cyclical nature of the path, and the *final* keyframe being conditioned on the *initial* observation. Views towards the end of the spin are, therefore, able to incorporate information from that given view (with low depth, in the sense of Sec. 3.3), which results in better generation quality. Next, we examine TSED on neighbouring views (see Fig. 5b, middle), where all methods perform relatively the same; in other words, consistency between adjacent frames is not strongly affected. However, this evaluation does not capture the loop inconsistency phenomenon, which will occur as a divergence between similar camera viewpoints with different conditioning histories. To analyze this scenario, we also compute TSED on the first and last generated frames of the cyclical spin motion (see Fig. 1 and [57]) Fig. 5b (right) shows that set-based sampling is dramatically more effective at generating cyclical views-sets (>90% vs. <40% matching). Qualitatively, the example shown in Fig. 1 shows a region visible in the given image that the model fails to maintain, causing it to change in the final view.

Table 2. Reconstruction metrics on stereo pairs, where ground-truth reference frames are available ("right eye" view).

Method	Short-term		Long-term	
	LPIPS ↓	PSNR ↑	LPIPS ↓	PSNR ↑
Std. Auto.	0.550	12.44	0.722	10.51
Group Sampling	**0.349**	**15.06**	**0.649**	**11.35**

4.3. Grouped sequential generation

Next, we consider NVS over sequences of groups of views, where views within a group cannot be naturally ordered; specifically, we consider trajectories of binocular stereo pairs. We create these trajectories by modifying the in-distribution trajectories used in Sec. 4.2, via treating it as the "right eye" adding a "left" one to generate a stereo pair for each view. For a simple baseline, we apply standard autoregressive sampling with a *zigzag* ordering, where the right and then the left views are sampled before repeating for the next stereo pair. Our set-based approach avoids imposing such an ordering by performing *grouped sampling* (a form of set-autoregression), implemented by sampling each stereo pair as a set, while conditioning on the previous pair.

Since we base our stereo trajectories on a real trajectory with ground-truth, we can perform reference-based evaluations on the *right* view of each generated stereo pair. Results in Tab. 2 are performed over short-term and long-term views, as in Sec. 4.2, which show that our grouped sampling method outperforms the autoregressive method.

We also evaluate the quality of the views over subsequent generations using FID. The FID results in Fig. 7 are arranged using the same zigzag ordering used for the simple baseline. Our grouped sampling is able to reduce the degradation of image quality compared to the simple autoregressive baseline.

Finally, we use TSED to evaluate consistency between generations. However, the lack of a natural order overall views requires careful selection of the pairs used for evaluation. We therefore consider two types of view pairs for TSED evaluations: same-sided and cross-sided. For same-sided evaluations, pairs of views from the same side of the stereo pairs (i.e., left or right), and adjacent in the sequence of pairs are considered. For cross-sided evaluations, pairs on the opposite sides of the stereo pairs, and adjacent in the sequence of pairs, are considered. The TSED results in Fig. 7 show that grouped (i.e., set-wise) generation is significantly more consistent, especially for the same-sided evaluations. This consistency can be observed qualitatively in Fig. 8. Overall, the set-based grouped method, which is more strongly constrained by multiview conditioning and does not impose an arbitrary ordering on the binocular pairs, results in better generations in terms of image quality and cross-frame consistency.
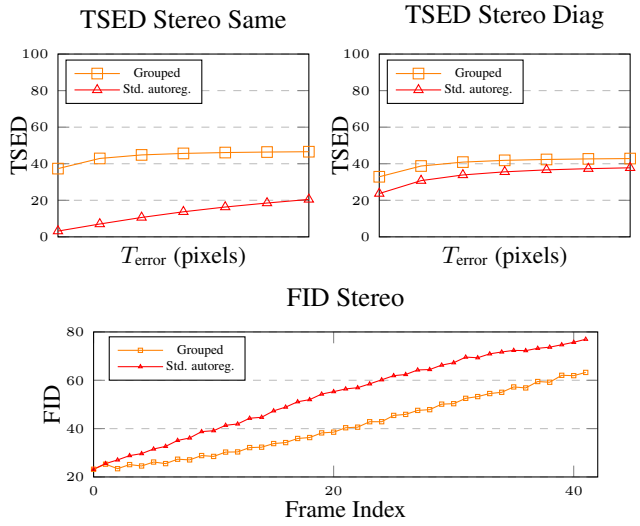

Figure 7. Upper row: TSED plots measuring inter-frame consistency between same-eye generations (left inset) and different-eye generations (right inset), across adjacent stereo pairs in time. Bottom inset: FID across time (ordered in the "zigzag" manner).
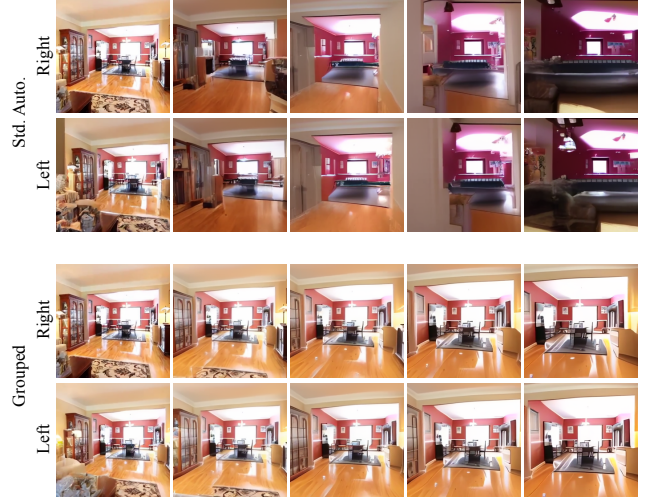

Figure 8. A qualitative example of a generated stereo pair using standard autoregressive and grouped sampling. Notice that the scene content diverges quickly when using standard autoregressive generation. Views progress from the left to the right columns.

5. Conclusion

In this paper, we proposed a set-based approach to the generative novel view synthesis (GNVS) problem. Not only are many camera trajectories of interest inherently difficult to order, but set-based generation may potentially alleviate the accumulation of errors in autoregressive generation. To this end, we devised a flexible set-to-set generative model which both conditions on and outputs *sets* of images, in a permutation-invariant manner. We evaluate the model us-

ing standard NVS metrics and datasets, obtaining improved image quality. We also demonstrated even larger improvements when generating particularly challenging view sets, including cyclic paths (which induce loop inconsistencies) and binocular trajectories (which are not naturally ordered). We believe that this approach can help mitigate common problems with image-based GNVS, and form the foundation for future GNVS techniques generally.

References

[1] Titas Anciukevicius, Zexiang Xu, Matthew Fisher, Paul Henderson, Hakan Bilen, Niloy J. Mitra, and Paul Guerrero. RenderDiffusion: Image diffusion for 3D reconstruction, inpainting and generation. *Proceedings of the IEEE Conference on Computer Vision and Pattern Recognition (CVPR)*, 2023. 2, 3

[2] Yasuhiro Aoki, Hunter Goforth, Rangaprasad Arun Srivatsan, and Simon Lucey. PointNetLK: Robust & efficient point cloud registration using PointNet. In *Proceedings of the IEEE Conference on Computer Vision and Pattern Recognition (CVPR)*, 2019. 3

[3] Shai Avidan and Amnon Shashua. Novel view synthesis in tensor space. In *Proceedings of the IEEE Conference on Computer Vision and Pattern Recognition (CVPR)*, 1997. 3

[4] Jonathan T Barron, Ben Mildenhall, Dor Verbin, Pratul P Srinivasan, and Peter Hedman. Zip-NeRF: Anti-aliased grid-based neural radiance fields. *arXiv preprint arXiv:2304.06706*, 2023. 3

[5] Miguel Ángel Bautista, Pengsheng Guo, Samira Abnar, Walter Talbott, Alexander T Toshev, Zhuoyuan Chen, Laurent Dinh, Shuangfei Zhai, Hanlin Goh, Daniel Ulbricht, Afshin Dehghan, and Joshua M. Susskind. GAUDI: A neural architect for immersive 3D scene generation. In *Neural Information Processing Systems (NeurIPS)*, 2022. 3

[6] Andreas Blattmann, Robin Rombach, Huan Ling, Tim Dockhorn, Seung Wook Kim, Sanja Fidler, and Karsten Kreis. Align your latents: High-resolution video synthesis with latent diffusion models. In *Proceedings of the IEEE Conference on Computer Vision and Pattern Recognition (CVPR)*, 2023. 3

[7] Nicolas Carion, Francisco Massa, Gabriel Synnaeve, Nicolas Usunier, Alexander Kirillov, and Sergey Zagoruyko. End-to-end object detection with transformers. In *Proceedings of the European Conference on Computer Vision (ECCV)*, 2020. 3

[8] Alexandre Carlier, Martin Danelljan, Alexandre Alahi, and Radu Timofte. DeepSVG: A hierarchical generative network for vector graphics animation. *Neural Information Processing Systems (NeurIPS)*, 2020. 3

[9] Eric R. Chan, Koki Nagano, Matthew A. Chan, Alexander W. Bergman, Jeong Joon Park, Axel Levy, Miika Aittala, Shalini De Mello, Tero Karras, and Gordon Wetzstein. GeNVS: Generative novel view synthesis with 3D-aware diffusion models. In *Proceedings of the International Conference on Computer Vision (ICCV)*, 2023. 2, 3

[10] SC Chan, Heung-Yeung Shum, and King-To Ng. Image-based rendering and synthesis. *IEEE Signal Processing Magazine*, 2007. 3

[11] Shenchang Eric Chen and Lance Williams. View interpolation for image synthesis. In *Proceedings of SIGGRAPH*, 1993. 3

[12] Florinel-Alin Croitoru, Vlad Hondru, Radu Tudor Ionescu, and Mubarak Shah. Diffusion models in vision: A survey. *IEEE Transactions on Pattern Analysis and Machine Intelligence (PAMI)*, 2023. 2

[13] Matt Deitke, Ruoshi Liu, Matthew Wallingford, Huong Ngo, Oscar Michel, Aditya Kusupati, Alan Fan, Christian Laforte, Vikram Voleti, Samir Yitzhak Gadre, Eli VanderBilt, Aniruddha Kembhavi, Carl Vondrick, Georgia Gkioxari, Kiana Ehsani, Ludwig Schmidt, and Ali Farhadi. Objaverse-XL: A universe of 10M+ 3D objects. *arXiv preprint arXiv:2307.05663*, 2023. 3

[14] Patrick Esser, Robin Rombach, and Bjorn Ommer. Taming transformers for high-resolution image synthesis. In *Proceedings of the IEEE Conference on Computer Vision and Pattern Recognition (CVPR)*, 2021. 6

[15] John Flynn, Michael Broxton, Paul Debevec, Matthew DuVall, Graham Fyffe, Ryan Overbeck, Noah Snavely, and Richard Tucker. DeepView: View synthesis with learned gradient descent. In *Proceedings of the IEEE Conference on Computer Vision and Pattern Recognition (CVPR)*, 2019. 3

[16] Kyle Gao, Yina Gao, Hongjie He, Dening Lu, Linlin Xu, and Jonathan Li. NeRF: Neural radiance field in 3D vision, a comprehensive review. *arXiv preprint arXiv:2210.00379*, 2022. 3

[17] Michal Geyer, Omer Bar-Tal, Shai Bagon, and Tali Dekel. Tokenflow: Consistent diffusion features for consistent video editing. *arXiv preprint arXiv:2307.10373*, 2023. 3

[18] Chenhang He, Ruihuang Li, Shuai Li, and Lei Zhang. Voxel set transformer: A set-to-set approach to 3D object detection from point clouds. In *Proceedings of the IEEE Conference on Computer Vision and Pattern Recognition (CVPR)*, 2022. 3

[19] Martin Heusel, Hubert Ramsauer, Thomas Unterthiner, Bernhard Nessler, and Sepp Hochreiter. GANS trained by a two time-scale update rule converge to a local Nash equilibrium. *Neural Information Processing Systems (NeurIPS)*, 2017. 6

[20] Jonathan Ho, Ajay Jain, and Pieter Abbeel. Denoising diffusion probabilistic models. *Neural Information Processing Systems (NeurIPS)*, 2020. 3, 6

[21] Jonathan Ho, Tim Salimans, Alexey Gritsenko, William Chan, Mohammad Norouzi, and David J Fleet. Video diffusion models. *Proceedings of the International Conference on Learning Representations (ICLR)*, 2022. 4

[22] Jinwoo Kim, Jaehoon Yoo, Juho Lee, and Seunghoon Hong. SetVAE: Learning hierarchical composition for generative modeling of set-structured data. In *Proceedings of the IEEE Conference on Computer Vision and Pattern Recognition (CVPR)*, 2021. 3

[23] Seung Wook Kim, Bradley Brown, Kangxue Yin, Karsten Kreis, Katja Schwarz, Daiqing Li, Robin Rombach, Antonio Torralba, and Sanja Fidler. NeuralField-LDM: Scene generation with hierarchical latent diffusion models. In *Proceedings of the IEEE Conference on Computer Vision and Pattern Recognition (CVPR)*, 2023. 3

[24] Stephane Laveau and Olivier D Faugeras. 3-D scene representation as a collection of images. In *Proceedings of the International Conference on Pattern Recognition (ICPR)*, 1994. 3

[25] Juho Lee, Yoonho Lee, Jungtaek Kim, Adam Kosiorek, Seungjin Choi, and Yee Whye Teh. Set transformer: A framework for attention-based permutation-invariant neural net-

works. In *Proceedings of the International Conference on Machine Learning (ICML)*, 2019. 3

[26] Andrew Liu, Richard Tucker, Varun Jampani, Ameesh Makadia, Noah Snavely, and Angjoo Kanazawa. Infinite nature: Perpetual view generation of natural scenes from a single image. In *Proceedings of the International Conference on Computer Vision (ICCV)*, 2021. 3

[27] Ruoshi Liu, Rundi Wu, Basile Van Hoorick, Pavel Tokmakov, Sergey Zakharov, and Carl Vondrick. Zero-1-to-3: Zero-shot one image to 3D object. In *Proceedings of the International Conference on Computer Vision (ICCV)*, 2023. 2, 3

[28] Shitong Luo and Wei Hu. Diffusion probabilistic models for 3D point cloud generation. In *Proceedings of the IEEE Conference on Computer Vision and Pattern Recognition (CVPR)*, 2021. 3

[29] Ben Mildenhall, Pratul P. Srinivasan, Matthew Tancik, Jonathan T. Barron, Ravi Ramamoorthi, and Ren Ng. NeRF: Representing scenes as neural radiance fields for view synthesis. In *Proceedings of the European Conference on Computer Vision (ECCV)*, 2020. 1, 3

[30] Weili Nie, Arash Vahdat, and Anima Anandkumar. Controllable and compositional generation with latent-space energy-based models. In *Neural Information Processing Systems (NeurIPS)*, 2021. 4

[31] Ryan Po, Wang Yifan, Vladislav Golyanik, Kfir Aberman, Jonathan T Barron, Amit H Bermano, Eric Ryan Chan, Tali Dekel, Aleksander Holynski, Angjoo Kanazawa, et al. State of the art on diffusion models for visual computing. *arXiv preprint arXiv:2310.07204*, 2023. 2

[32] Charles R Qi, Hao Su, Kaichun Mo, and Leonidas J Guibas. PointNet: Deep learning on point sets for 3D classification and segmentation. In *Proceedings of the IEEE Conference on Computer Vision and Pattern Recognition (CVPR)*, 2017. 3

[33] Charles Ruizhongtai Qi, Li Yi, Hao Su, and Leonidas J Guibas. PointNet++: Deep hierarchical feature learning on point sets in a metric space. *Neural Information Processing Systems (NeurIPS)*, 2017. 3

[34] Siamak Ravanbakhsh, Jeff Schneider, and Barnabas Poczos. Deep learning with sets and point clouds. *arXiv preprint arXiv:1611.04500*, 2016. 3

[35] Xuanchi Ren and Xiaolong Wang. Look outside the room: Synthesizing a consistent long-term 3D scene video from a single image. In *Proceedings of the IEEE Conference on Computer Vision and Pattern Recognition (CVPR)*, 2022. 2, 3, 5, 6

[36] Robin Rombach, Patrick Esser, and Björn Ommer. Geometry-free view synthesis: Transformers and no 3D priors. In *Proceedings of the International Conference on Computer Vision (ICCV)*, 2021. 2, 3, 5, 6

[37] Robin Rombach, Andreas Blattmann, Dominik Lorenz, Patrick Esser, and Björn Ommer. High-resolution image synthesis with latent diffusion models. In *Proceedings of the IEEE Conference on Computer Vision and Pattern Recognition (CVPR)*, 2022. 4, 6

[38] Olaf Ronneberger, Philipp Fischer, and Thomas Brox. U-Net: Convolutional networks for biomedical image segmentation. In *Proceedings of the International Conference on Medical Image Computing and Computer Assisted Intervention (MICCAI)*, 2015. 4

[39] Mehdi S. M. Sajjadi, Henning Meyer, Etienne Pot, Urs Bergmann, Klaus Greff, Noha Radwan, Suhani Vora, Mario Lucic, Daniel Duckworth, Alexey Dosovitskiy, Jakob Uszkoreit, Thomas Funkhouser, and Andrea Tagliasacchi. Scene representation transformer: Geometry-free novel view synthesis through set-latent scene representations. In *Proceedings of the IEEE Conference on Computer Vision and Pattern Recognition (CVPR)*, 2022. 3, 5, 13

[40] Paul-Edouard Sarlin, Daniel DeTone, Tomasz Malisiewicz, and Andrew Rabinovich. SuperGlue: Learning feature matching with graph neural networks. In *Proceedings of the IEEE Conference on Computer Vision and Pattern Recognition (CVPR)*, 2020. 3

[41] Daniel Scharstein. Stereo vision for view synthesis. In *Proceedings of the IEEE Conference on Computer Vision and Pattern Recognition (CVPR)*, 1996. 3

[42] Nimrod Segol and Yaron Lipman. On universal equivariant set networks. *Proceedings of the International Conference on Learning Representations (ICLR)*, 2020. 3

[43] Steven M Seitz and Charles R Dyer. Physically-valid view synthesis by image interpolation. In *ICCV Workshop on Representation of Visual Scenes*, 1995. 3

[44] Harry Shum and Sing Bing Kang. Review of image-based rendering techniques. In *Visual Communications and Image Processing*. SPIE, 2000. 3

[45] Jascha Sohl-Dickstein, Eric Weiss, Niru Maheswaranathan, and Surya Ganguli. Deep unsupervised learning using nonequilibrium thermodynamics. In *Proceedings of the International Conference on Machine Learning (ICML)*, 2015. 3

[46] Jiaming Song, Chenlin Meng, and Stefano Ermon. Denoising diffusion implicit models. *arXiv preprint arXiv:2010.02502*, 2020. 3

[47] Stanislaw Szymanowicz, Christian Rupprecht, and Andrea Vedaldi. Viewset diffusion: (0-)image-conditioned 3D generative models from 2D data. In *Proceedings of the International Conference on Computer Vision (ICCV)*, 2023. 2, 3, 5

[48] Matthew Tancik, Pratul Srinivasan, Ben Mildenhall, Sara Fridovich-Keil, Nithin Raghavan, Utkarsh Singhal, Ravi Ramamoorthi, Jonathan Barron, and Ren Ng. Fourier features let networks learn high frequency functions in low dimensional domains. *Neural Information Processing Systems (NeurIPS)*, 2020. 5

[49] Ayush Tewari, Tianwei Yin, George Cazenavette, Semon Rezchikov, Joshua B. Tenenbaum, Frédo Durand, William T. Freeman, and Vincent Sitzmann. Diffusion with forward models: Solving stochastic inverse problems without direct supervision. *Neural Information Processing Systems (NeurIPS)*, 2023. 2, 3, 5

[50] Hung-Yu Tseng, Qinbo Li, Changil Kim, Suhib Alsisan, Jia-Bin Huang, and Johannes Kopf. Consistent view synthesis

with pose-guided diffusion models. In *Proceedings of the IEEE Conference on Computer Vision and Pattern Recognition (CVPR)*, 2023. 2, 3, 5

[51] Qianqian Wang, Zhicheng Wang, Kyle Genova, Pratul P Srinivasan, Howard Zhou, Jonathan T Barron, Ricardo Martin-Brualla, Noah Snavely, and Thomas Funkhouser. IBRNet: Learning multi-view image-based rendering. In *Proceedings of the IEEE Conference on Computer Vision and Pattern Recognition (CVPR)*, 2021. 6

[52] Daniel Watson, William Chan, Ricardo Martin-Brualla, Jonathan Ho, Andrea Tagliasacchi, and Mohammad Norouzi. Novel view synthesis with diffusion models. *Proceedings of the International Conference on Learning Representations (ICLR)*, 2023. 2, 3, 4, 5

[53] Yiheng Xie, Towaki Takikawa, Shunsuke Saito, Or Litany, Shiqin Yan, Numair Khan, Federico Tombari, James Tompkin, Vincent Sitzmann, and Srinath Sridhar. Neural fields in visual computing and beyond. In *Computer Graphics Forum*, 2022. 3

[54] Han-Jia Ye, Hexiang Hu, De-Chuan Zhan, and Fei Sha. Few-shot learning via embedding adaptation with set-to-set functions. In *Proceedings of the IEEE Conference on Computer Vision and Pattern Recognition (CVPR)*, 2020. 3

[55] Senthil Yogamani, Ciarán Hughes, Jonathan Horgan, Ganesh Sistu, Padraig Varley, Derek O'Dea, Michal Uricár, Stefan Milz, Martin Simon, Karl Amende, et al. WoodScape: A multi-task, multi-camera fisheye dataset for autonomous driving. In *Proceedings of the International Conference on Computer Vision (ICCV)*, 2019. 3

[56] Alex Yu, Vickie Ye, Matthew Tancik, and Angjoo Kanazawa. pixelNeRF: Neural radiance fields from one or few images. In *Proceedings of the IEEE Conference on Computer Vision and Pattern Recognition (CVPR)*, 2021. 3

[57] Jason J. Yu, Fereshteh Forghani, Konstantinos G. Derpanis, and Marcus A. Brubaker. Long-term photometric consistent novel view synthesis with diffusion models. In *Proceedings of the International Conference on Computer Vision (ICCV)*, 2023. 2, 3, 4, 5, 6, 7, 13, 14

[58] Manzil Zaheer, Satwik Kottur, Siamak Ravanbakhsh, Barnabas Poczos, Russ R Salakhutdinov, and Alexander J Smola. Deep sets. *Neural Information Processing Systems (NeurIPS)*, 2017. 3

[59] Richard Zhang, Phillip Isola, Alexei A Efros, Eli Shechtman, and Oliver Wang. The unreasonable effectiveness of deep features as a perceptual metric. In *Proceedings of the IEEE Conference on Computer Vision and Pattern Recognition (CVPR)*, 2018. 6

[60] Yan Zhang, Jonathon Hare, and Adam Prugel-Bennett. Deep set prediction networks. *Neural Information Processing Systems (NeurIPS)*, 2019. 3

[61] Yan Zhang, Jonathon Hare, and Adam Prügel-Bennett. FSPool: Learning set representations with featurewise sort pooling. In *Proceedings of the International Conference on Learning Representations (ICLR)*, 2019. 3

[62] Yan Zhang, David W Zhang, Simon Lacoste-Julien, Gertjan J Burghouts, and Cees GM Snoek. Multiset-equivariant set prediction with approximate implicit differentiation. *Proceedings of the International Conference on Learning Representations (ICLR)*, 2022. 3

[63] Tinghui Zhou, Richard Tucker, John Flynn, Graham Fyffe, and Noah Snavely. Stereo magnification. *ACM Transactions on Graphics*, 2018. 6

Appendix A. Camera Ray Encoding

To provide our model with access to the camera geometry, we adopt the ray representation used in previous works [39, 57]. Given the intrinsic, $\mathbf{K}$, and the extrinsic matrix, $[\mathbf{R}|\mathbf{t}]$, of a camera, the projection matrix is defined as $\mathbf{P} = \mathbf{K}[\mathbf{R}|\mathbf{t}]$. The ray $\mathbf{r}_{u,v} = (\boldsymbol{\tau}, \mathbf{d}_{u,v})$ at pixel coordinates (u, v) is composed of the camera center $\boldsymbol{\tau} = -\mathbf{R}^{-1}\mathbf{t}$, and normalized direction $\mathbf{d}_{u,v}$. The unnormalized ray direction is given by:

$$\bar{\mathbf{d}}_{u,v} = \mathbf{R}^{-1}\mathbf{K}^{-1}\begin{bmatrix} u & v & 1 \end{bmatrix}^{\top}. \tag{9}$$

The rays, $\mathbf{r}$, are frequency encoded into their final representation, $\mathcal{R}$, which is then used to condition the model:

$$\mathcal{R} = \left[\sin(f_1\pi\mathbf{r}), \cos(f_1\pi\mathbf{r}), \ldots, \sin(f_K\pi\mathbf{r}), \cos(f_K\pi\mathbf{r})\right], \tag{10}$$

where K frequencies are used, which increment in frequency by powers of two.

Appendix B. Generating Large Sets of Unordered Views

In general, views within a set do not necessarily have a single natural ordering or any at all. In cases where the ordering may be completely arbitrary, a heuristic based on the proximity of camera poses can be used to order the views for sampling. Next, we describe one such simple heuristic.

Given a set of N camera poses, we iteratively grow a set of keyframes, Ω, as a small subset of all the frames. Starting with the pose of the given view, k_1, we choose the next keyframe in Ω as a view that is not already a keyframe, and is furthest from any of the existing keyframes:

$$k_i = \operatorname*{arg\,max}_{\mathbf{c}_r \notin \{k_1, \ldots k_{i-1}\}} \min_{\mathbf{c}_s \in \{k_1, \ldots k_{i-1}\}} d(\mathbf{c}_r, \mathbf{c}_s), \tag{11}$$

where k_i is the ith selected keyframe, and $d(\mathbf{c}_r, \mathbf{c}_s)$ quantifies a distance between the cameras. This heuristic is chosen to spread the keyframes out while having high coverage of the space occupied by the views. The remaining views are used as in-between frames with a generation order defined in a similar manner to the keyframe selection method in Eq. 11. The in-between frames are conditioned on a subset of the closest views that have already been generated (these may not necessarily be keyframes).

Appendix C. Additional Results: Out-of-Distribution - Orbit and Hop

Previous work [57] also defined additional out-of-distribution evaluation trajectories: spin, orbit and hop. All these trajectories are atypical of the ones found in the training data and are considered more challenging than the in-distribution trajectories used in the standard evaluations.

In the main paper, we include results on spin due to its unique cyclical structure, which is highly suited for generation in unordered settings, the focus of our paper. While our method does not directly address general out-of-distribution trajectories, we include the evaluations of both hop and orbit here for completeness. These trajectories are particularly challenging for our keyframed sampling method, and yield lower consistency in terms of TSED, shown in Fig. 9.
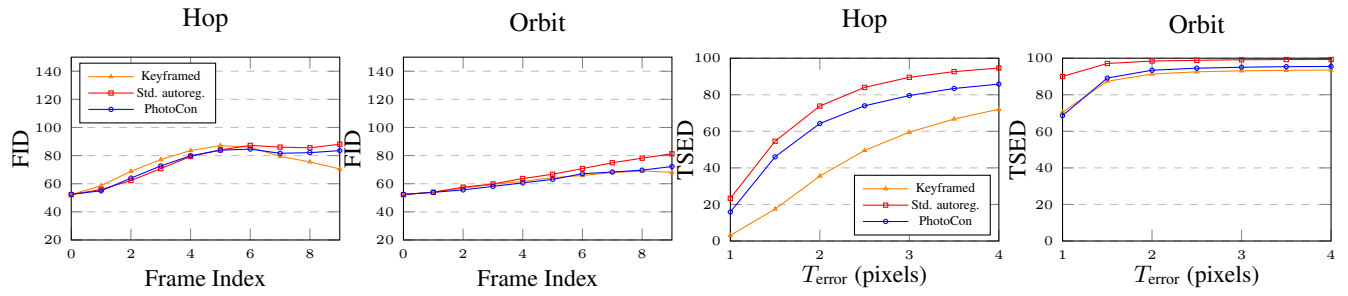
13

Figure 9. FID and TSED plots on RealEstate10K for hop and orbit trajectories used in previous work [57]. The atypical camera motions in these trajectories are challenging when generating the keyframes which are far apart.